Quantal Potential Fields around Individual Active Zones of Amphibian Motor-Nerve Terminals

M. R. Bennett,* L. Farnell,[†] W. G. Gibson,[†] G. T. Macleod,* and P. Dickens*

*The Neurobiology Laboratory, Department of Physiology, Institute for Biomedical Research and [†]The School of Mathematics and Statistics, University of Sydney, New South Wales 2006, Australia

ABSTRACT　The release of a quantum from a nerve terminal is accompanied by the flow of extracellular current, which creates a field around the site of transmitter action. We provide a solution for the extent of this field for the case of a quantum released from a site on an amphibian motor-nerve terminal branch onto the receptor patch of a muscle fiber and compare this with measurements of the field using three extracellular electrodes. Numerical solution of the equations for the quantal potential field in cylindrical coordinates show that the density of the field at the peak of the quantal current gives rise to a peak extracellular potential, which declines approximately as the inverse of the distance from the source at distances greater than about 4 μm from the source along the length of the fiber. The peak extracellular potential declines to 20% of its initial value in a distance of about 6 μm, both along the length of the fiber and in the circumferential direction around the fiber. Simultaneous recordings of quantal potential fields, made with three electrodes placed in a line at right angles to an FM1–43 visualized branch, gave determinations of the field strengths in accord with the numerical solutions. In addition, the three electrodes were placed so as to straddle the visualized release sites of a branch. The positions of these sites were correctly predicted on the basis of the theory and independently ascertained by FM1–43 staining of the sites. It is concluded that quantal potential fields at the neuromuscular junction that can be measured with available recording techniques are restricted to regions within about 10 μm of the release site.

INTRODUCTION

Recording the electrical signs of quantal secretion at visualized release sites with either loose-patch or sharp electrodes was initially carried out at the amphibian neuromuscular junction (Bennett et al., 1986). Since then, loose-patch recordings have been made from single visualized synapses formed by sympathetic varicosities on smooth muscle cells (Lavidis and Bennett, 1992), sympathetic boutons on ganglion cells (Bennett et al., 1997), and at boutons on hippocampal neurons (Forti et al., 1997). However, there is no detailed analytical or numerical solution that describes how current flows in the extracellular space about a synapse upon the release of a quantum and allows for comparison with experiment. There is also no guide to the extent of distortion of this quantal current field by glial cells partially enveloping the synapse or by the recording electrode itself.

Several investigations have been made into the extent of the extracellular currents and potentials due to action potential conduction along an axon or muscle fiber in a volume conductor (Clark and Plonsey, 1968; Malmivuo and Plonsey, 1995; Stephanova et al., 1989; Trayanova et al., 1990); others have considered the generation of action potentials in axons or axon bundles by stimulation from external electrodes (Rattray, 1986, 1987, 1989; Altman and Plonsey, 1988), but none of these allow for determination of the quantal current field. Solutions for the interior potential

and current flow resulting from current injection into spherical cells have been obtained (Eisenberg and Johnson, 1970; Engel et al., 1972; Pickard, 1971a,b), but in all these cases the exterior is assumed to be at Earth potential. Two papers (Peskoff and Eisenberg, 1975; Peskoff and Ramirez, 1975) do consider the external field, but only for the purpose of showing that the position of an external sink and the conduction of the external fluid have little effect on the membrane potential. In the case of motor-nerve terminals, for which most experimental evidence is available, the problem that requires solution relates to charge spread when applied at a point on a cable of non-negligible diameter in a volume conductor, so that current flows both transversely and along the length of the cylindrical cable. A cylindrical version of the cable theory has recently been solved by an extension of standard linear theory (Hodgkin and Rushton, 1946; Tuckwell, 1988) for the case in which current flow in the volume conductor is restricted to an annulus about a cylinder (Thomson et al., 1995). However, it is not possible to solve for the quantal potential field without determination of current flow in the volume conductor. The present work provides a solution to this problem, enabling evaluation of the quantal potential field.

Following the discovery of spontaneous miniature endplate potentials (MEPPs) by Fatt and Katz (1952) and their analysis as quantal units of transmitter release (del Castillo and Katz, 1954), attempts were made to determine the spatial origin of these within the endplate using one or two extracellular electrodes (del Castillo and Katz, 1956; Katz and Miledi, 1965a,b). The conclusion reached was that the extracellular current generating the MEPP (namely the miniature endplate current, or MEPC) was attenuated to one-

quarter of its amplitude at a site about 10 μm in the longitudinal direction from the source; thus, if an electrode was more than 15–20 μm from the source, then the MEPC was not recorded at all (Katz and Miledi, 1965a,b; Wernig, 1975, 1976; Bennett and Lavidis, 1982). These results were later confirmed on visualized terminal branches that were in relative isolation from other branches within a single end-plate. Furthermore, it was shown that the MEPC declines to less than one quarter in a distance of about 10 μm in the transverse direction from the source (Bennett et al., 1986). Techniques have now been introduced involving the use of three external electrodes to record the quantal potential field and a triangulation algorithm applied to the recordings for the purposes of determining the location of the source of the field (Zefirov et al., 1990, 1995). This approach has recently been extended to obtain the amplitude of the quantal potential at the source (Macleod et al., 1999). Application of this algorithm requires a knowledge of the relation between the quantal potential field strength at different distances from the source. This relation is obtained in the present work and compared with experimental values of the quantal potential field strength about different visualized quantal release sites along amphibian motor-nerve terminal branches.

METHODS

Theoretical

The muscle fiber is taken to be a cylinder of infinite length with circular cross-section of radius a. Let $V = V(r, t)$ be the deviation from resting potential at time t at the point r; then for r not on the membrane, because there are no current sources or sinks, V satisfies Laplace's equation:

$$\nabla^2 V = 0. \qquad (1)$$

In cylindrical polars this is

$$\frac{1}{r}\frac{\partial}{\partial r}\left(r\frac{\partial V}{\partial r}\right) + \frac{1}{r^2}\frac{\partial^2 V}{\partial \theta^2} + \frac{\partial^2 V}{\partial z^2} = 0, \quad r \neq a, \qquad (2)$$

where the z-axis is taken along the axis of the cylinder. If synaptic conductance occurs at the point $(r, \theta, z) = (a, 0, 0)$ then the boundary condition at the membrane is (see, e.g., Peskoff and Eisenberg, 1975)

$$\frac{1}{R_i}\frac{\partial V}{\partial r}\bigg|_{r=a-} = \frac{1}{R_e}\frac{\partial V}{\partial r}\bigg|_{r=a+} = -\frac{V_m}{R_m} - C_m\frac{\partial V_m}{\partial t}$$

$$+ I(t)\frac{1}{a}\delta(\theta)\delta(z), \quad r = a, \qquad (3)$$

where R_m (Ωcm^2) is the membrane resistance, C_m (F cm^{-2}) is the membrane capacitance, R_i (Ωcm) and R_e (Ωcm) are respectively the intracellular and extracellular resistivities, $V_m = V(r = a-) - V(r = a+)$ is the membrane potential, $I(t)$ is the current that mimics synaptic transmission and $\delta(\theta)\delta(z)$ are Dirac delta functions indicating that this current is applied at the point $\theta = 0$, $z = 0$ on the membrane. The physical interpretation of the boundary condition (ref{bc}) is that the normal component of current density is continuous across the membrane and is equal to the sum of the resistance and capacitance currents crossing the membrane, plus a term representing the effective current due to the synaptic conductance change. This term is equivalent to a current source $I(t)$ at $(r, \theta, z) = (a-, 0, 0)$ and

a current sink of equal strength at $(a+, 0, 0)$. This method of treating a synaptic conductance change is valid provided the resulting change in membrane potential is small. The form assumed for this current is a sum of exponentials:

$$I(t) = I_0(e^{-\alpha t} - e^{-\beta t}), \qquad (4)$$

where I_0, α, and β are constants. The other boundary conditions required are on r and z. If the muscle fiber is in an infinite volume conductor this is simply that $V \rightarrow 0$ as $r \rightarrow \infty$. If the fiber is enclosed in another nonconducting coaxial cylinder of radius $b > a$, the condition is that there is no current flow in the radial direction across this outer cylinder, so $\partial V/\partial r = 0$ for $r = b$. Similarly, for a cylinder of infinite length, $V \rightarrow 0$ as $z \rightarrow \pm\infty$, and for one of finite length with sealed ends it is $\partial V/\partial z = 0$ at the ends.

Eqs. 2 and 3 are solved numerically, using a three-dimensional cylindrical polar mesh with grid spacings δr, $r\delta\theta$, and δz. Temporal updating on this mesh is done using the leap-frog algorithm that we have employed in previous calculations of a similar nature (Bennett et al., 1993, 1999; Bennett and Gibson, 1995; Henery et al., 1997). Grid spacings used were about 1 μm near the source. However, because the potential falls off slowly, particularly parallel to the cylinder axis (z-direction), it was necessary to scale the mesh so that the grid size increased with distance from the source; in practice, a cubic scaling was found to give good accuracy while keeping the number of grid points within manageable bounds.

The use of a point source in Eq. 3 means that the exact solution $V(r, \theta, z)$ is singular (infinite) at the source point $(r, \theta, z) = (a, 0, 0)$. The numerical solution does not become infinite, but does attain unrealistically large values close to the source. This is clearly unphysical, being a consequence of the use of a point source rather than an extended source. It is therefore important to estimate the minimum distance for which the solution is still physically meaningful. This is investigated in the Appendix; the conclusion is that for distances of at least 1 mesh point away from the source the solution is meaningful. For the grid spacing used (about 1 μm near the source) this does not cause problems, as the measuring electrodes are always a minimum of several microns away from the point of synaptic transmission.

Two modifications were made to the basic program. The first was to allow for the nerve terminal together with its Schwann cell sheath. This was assumed to have a diameter of about 2 μm, to lie on the surface of the muscle fiber covering the release point, and to run the full length of the fiber. To allow for this, the appropriate nodes were removed from the integration mesh; specifically, the nodes at $r = (a + 1)$ μm, $\theta = -2.29°$, $0°$, $2.29°$, and all z.

A second modification was to take into account the effect of the T-tubules in the muscle fiber membrane by adding an extra series resistance and capacitance in addition to the usual membrane resistance and capacitance (Hodgkin and Nakajima, 1972a; Adrian and Almers, 1973; van der Kloot and Cohen, 1985). Details are not given, because it was found that the difference caused was small and did not alter any of the conclusions reached on the basis of the simpler model.

Parameter values

Quantal currents were taken as possessing a time to peak of 200 μs, an exponential decay time of 0.9 ms, and a maximum amplitude of 5 nA (at a temperature of 25°C; see Gage and Armstrong, 1968; Magleby and Stevens, 1972), leading to the values for I_0, α, and β in Table 1. The typical size of the potentials generated near the source of the quantal current fields in the present work was about 300 μV with the quantal transmembrane potentials at about 500 μV (Katz and Thesleff, 1957). The value of R_m (including both the surface membrane and the transverse tubular system) was 5000 Ωcm^2 (Katz, 1966; Hodgkin and Nakajima, 1972a), with an R_i of 80 Ωcm (Katz, 1966; Hodgkin and Nakajima, 1972a) and R_e of 60 Ωcm (Katz, 1966) and a membrane capacity of 1 μF cm^{-2} (Katz, 1966; Hodgkin and Nakajima, 1972b; if the transverse tubular system is included this is about 6 μF cm^{-2} for a fiber diameter of about 50 μm).

TABLE 1 Values of parameters used

Quantity	Symbol	Value
Synaptic current (Eq. 4)	I_0	6.797 nA
	α	1.111 ms^{-1}
	β	13.655 ms^{-1}
Membrane resistivity	R_m	5000 Ω cm^2
Membrane capacitance	C_m	1 μF cm^{-2}
Intracellular resistivity	R_i	80 Ω cm
Extracellular resistivity	R_e	60 Ω cm
Muscle fiber radius	a	25 μm

EXPERIMENTAL

All experiments were performed on the iliofibularis muscle or the *m.ext.l.dig.IV* muscle of the toad *Bufo marinus*. Animals were sacrificed by double pithing.

Standard fluorescence microscopy and image processing

The organ bath was constantly perfused at a rate of 3 ml per minute with frog Ringer: NaCl, 111.2 mM; KCl, 2.5 mM; NaH$_2$PO$_4$2H$_2$O, 1.5 mM; NaHCO$_3$, 16.3 mM; glucose, 7.8 mM; MgCl$_2$ 1.2 mM; bubbled with a gas mixture of 95% O$_2$/5% CO$_2$. [Ca^{2+}]$_0$ was 0.4 mM for all electrophysiological experiments and 1.8 mM for all procedures involving labeling with FM1−43. Temperature was maintained at 20°C to 22°C. Motor-nerve terminals were labeled with FM1−43 (Betz et al., 1992) by bathing the preparation in 2 μM FM1−43 in a modified Ringer solution (53.7 mM NaCl, 60 mM KCl) for 5 min. The preparation was washed for a minimum of 30 min before images were captured. Transillumination using a 50 W incandescent light source was used alternately with epi-illumination from a 100 W mercury arc lamp. An Olympus Fluorescein filter set was used to excite FM1−43 fluorescence, which was observed using a WV-BP310 Panasonic camera fitted to a BHT Olympus microscope with an Olympus 40 X water immersion objective (0.7 NA). Photo damage was minimized by stopping down the aperture iris diaphragm and inserting a 50% NDF in the excitation light path. Images were acquired using a Scion Corp LG3 frame-grabber. Pixellation of images was constant at 7.45 pixels per μm.

Electrophysiology

Electrophysiological recordings were made using either three or four microelectrodes in various configurations. The tips of extracellular electrodes were heat polished to a final inner diameter of 0.5 to 1.5 μm and then filled with 2 M NaCl. The intracellular electrode was filled with 3 M KCl and yielded a resistance of approximately 20 MΩ. Microelectrodes' tips were placed in two different configurations with respect to terminal branches: one case involved placing the electrodes at the points of a rough equilateral triangle no more than 8 μm apart while straddling a nerve terminal branch; in the other case, the electrodes were placed in a line at right angles to the terminal branch, with electrodes no more than 4 μm apart and the electrode closest to the branch no more than 4 μm distant from it. Placements of the extracellular electrodes observed through transillumination were made relative to a superimposed image of the FM1−43 stained nerve terminal and their final positions relative to the FM1−43 blobs were checked using epifluorescence. When the intracellular electrode was used, the muscle cell was impaled after all extracellular electrodes were in place, and both transillumination and epifluorescence were used to record any relative movements. A video record of the muscle surface and electrodes was made throughout the period of electrophysiological recording using a low level of transillumination. A 10-nA negative current was injected through each electrode while it was in recording position both before and after recording to check that the tip resistances had remained the same. A separate Axoclamp-2A amplifier was used for each electrode. Data were collected using a MacLab/4s data acquisition system, low pass filtered at 5 kHz and digitized at 20 kHz. All negative going events that were discernible by eye were measured using Igor Pro. For a set of amplitudes to be accepted as corresponding to the same quantal event, they were required to occur within 0.5 ms of each other, and all amplitudes were required to be >2 S.D. of the noise amplitude. Recordings were rejected for any one of the following reasons: changes in the bright-field or fluorescence appearance of the terminal; bursting behavior, although a consistently high level of spontaneous release was accepted; movement of either an electrode tip or the terminal branch by more than 1 μm during the period of recording.

Determination of current source locations

Data on the relative positions of the microelectrode tips and the recorded amplitude of events from each electrode allows the calculation of coordinates for the postsynaptic site of current generation for each event relative to the electrode tips. For the triangular configuration of electrodes, Zefirov et al. (1990) derived a system of equations that provide for a geometric construction of two overlapping circles in a rectangular coordinate system whose points of intersection define two mathematical solutions for each event. The equations (Eq. 11 in Zefirov et al., 1990) were built into an Excel spreadsheet that calculated the equations of the circles and solved for the points of intersection from the data for each event. It was taken that the voltage attenuates as the reciprocal of the distance from the site of quantal current generation, as shown in the theoretical section below.

For each event, the computerized algorithm provided two theoretical solutions and an amplitude based on the location of each. If we accept the mathematical solutions closest to the center of the three electrodes for every event, the am-

plitudes associated with these solutions will be the smallest amplitudes. Not all of the solutions in this group will be correct, as some of the events detected will have been events with a large amplitude outside the triangle defined by the electrodes. However, the correct amplitude will be determined for all events that occurred within the electrodes, some of which will be large amplitude events. The rejection criterion is as follows: if for each event, the amplitude associated with one of the mathematical solutions is >2 S.D. above the mean of the smallest amplitudes, that solution can be rejected as being improbable; if the other solution has an amplitude below this value, it can be accepted. If neither or both amplitudes are above this value, both solutions, and hence the event, is rejected. It is important to remember that most of the events, because of the small radius of detection of each electrode, are likely to have occurred within the electrodes.

The validity of this procedure was tested by using a fourth microelectrode to record the quantal events intracellularly at a location within 20 μm of the three extracellular electrodes. All movements of the preparation and electrode tips during the period of recording were corrected for by the computerized algorithm. The video record was used to confirm that electrode or preparation drift was uniform over the recording period. Numerous simulated data sets were processed to test the ability of the algorithm to reproduce two-dimensional maps, calculate the correct amplitude for events, and correct for terminal and electrode drift. Such simulations also allowed determinations of the quality of the spatial resolution, which is about 0.36 μm (see Fig. 3 in Macleod et al., 1999).

RESULTS

Theoretical

Numerical solutions for the distribution of current in the extracellular space about the site of a quantal release onto a muscle fiber of 50 μm diameter show that the current density falls off rapidly in the longitudinal direction (the z coordinate) at the surface of the fiber along a line that passes through the site of quantal release (that is, the θ coordinate equals zero). The current density is very low at z values of about 10 μm at different times during the increase and decrease in this current field that accompanies the actions of the quantum on the fiber. Determination of the current density in the circumferential direction around the fiber from the site of quantal release shows that it also falls off rapidly with θ. Quantitative determinations of the transmembrane currents and voltages arising during a quantal event were ascertained. The time course of the transmembrane potential (V_m) and current (I_m) changes at different distances along the fiber from the site of quantal release are given in Fig. 1, A and B, for $\theta = 0$. The peak values of the transmembrane potential falls off approximately exponen-

tially with distance along the length of the fiber, at $\theta = 0$, with a length constant of about 1700 μm (Fig. 1 C). The peak value of the transmembrane current falls even more rapidly with distance, though not exponentially (Fig. 1 D). In the circumferential direction the peak of the transmembrane potential falls to an approximately constant value at $\theta = 60°$ (Fig. 1 E) as does that of the transmembrane current density (Fig. 1 F).

Quantitative determinations were also made of the extracellular voltages arising during a quantal event (Fig. 2) in order to compare the predictions of the numerical model with the experimental determinations of the size of the extracellular quantal voltage fields using different configurations of three extracellular electrodes (see below). It was therefore necessary to calculate the size of the fields for a range of values of the cylindrical coordinates used. Fig. 2 gives the quantitative values for the size of the peak extracellular quantal voltages (V_e) along the length of the fiber for different heights above the surface of the muscle (h), in the range from 0 to 6.38 μm (Fig. 2 B). Also given are the values for the size of the peak extracellular quantal voltage for different displacements in the circumferential direction (θ) and for different heights above the surface of the fiber h (Fig. 2 C). There is a steep decrease in V_e, of about 85%, as z, $a\theta$, and h independently increase in the range 1 to 6.4 μm about the origin (Fig. 2, B and C).

The details of how the extracellular quantal voltage changes within 50 μm of a quantal release, both in the longitudinal and circumferential directions, are given for the surface of the muscle fiber in Fig. 3 A and for positions 1 μm above the surface of the fiber in Fig. 3 C, using log-log coordinates. At the surface of the fiber (Fig. 3 A), the extracellular voltage declines almost linearly in these coordinates for z greater than about 4 μm and for θ less than about 5° (corresponding to a distance of about 2.2 μm). Furthermore, this decline has a gradient close to -1 (the exact gradient of -1 is given by the fine broken lines in Fig. 3), indicating that in this range the extracellular potential declines approximately as the inverse of the distance from the source. A similar, approximately linear range is obtained when recordings are made about 1 μm above the surface of the fiber (Fig. 3 C). If a linear relation of gradient -1 in log-log coordinates is to be assumed for the interpretation of the measurements of extracellular quantal voltages, then it is important to maintain the extracellular recording electrodes at <1 μm above the surface of the muscle fiber if possible, without touching it, and for electrodes to be positioned at least 4 μm from the quantal source.

The calculations above do not take into account the fact that quantal release sites are on terminal branches that are mostly encased in Schwann cell. In this case, the current generated by the quantum of transmitter acting on the receptor patch beneath the release site will be excluded from the volume occupied by the overlying terminal branch and associated Schwann cell. To determine the effects of this,
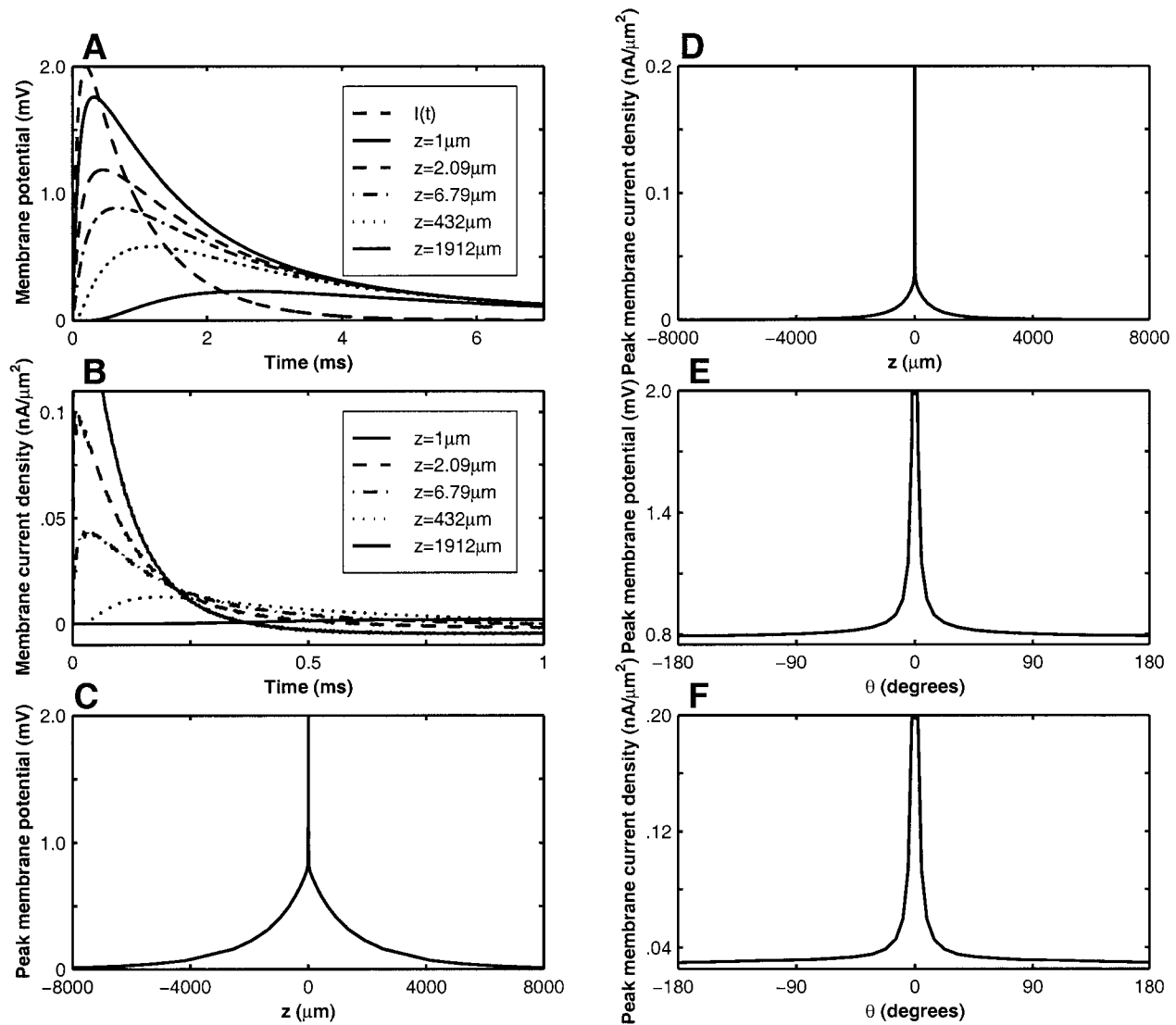
FIGURE 1   Transmembrane quantal potentials and currents following a quantal release at time t = 0 at the point $\theta = 0$, $z = 0$. A and B give, respectively, the membrane potential V_m and membrane current density I_m (calculated as $I_m = V_m/R_m + C_{mdVm}/dt$) as functions of time for $\theta = 0$ and for selected values of z. Also shown in A is the input current $I(t)$ (*upper broken line*); no scale is given for $I(t)$, but its peak is 5 nA. C and D give, respectively, the peak values attained by V_m and by I_m at distance z along the length of the fiber for $\theta = 0$. E and F give, respectively, the peak values attained by V_m and by I_m at angle θ around the fiber for $z = 0$. In all cases, potentials and currents are shown at points no closer than 1 μm to the source; at closer distances the calculated values are not physically meaningful because of the singularity at the source point (see Appendix).

current was excluded from a cylindrical volume 2 μm in diameter positioned with center at $\theta = 0$ and $h = 1$ μm. The distortion of the extracellular quantal current lines about the release site at different times after the release of a quantum was determined. These distortions have the effect of slightly increasing the size of the quantal potential field up to 4 μm from the source and of maintaining the field strength without much diminution within this 4-μm range (compare Fig. 3, B and D, with Fig. 3, A and C). However, a nearly linear relation of gradient -1 between the logarithm of the extracellular quantal potential and the logarithm of the distance from the source still remains beyond about 4 μm from the source in the longitudinal direction for θ values less than

about 9° and for heights above the surface of between 0 and 1 μm (Fig. 3, B and D). There is little difference in the size of the voltage field for distances greater than about 10 μm if allowance is made for the exclusion of the current from the volume occupied by the terminal branch and its encasing Schwann (compare Fig. 4 with Fig. 2).

Experimental

The quantal potential fields were measured with different configurations of three external microelectrodes about terminal branches that were visualized by prior staining with
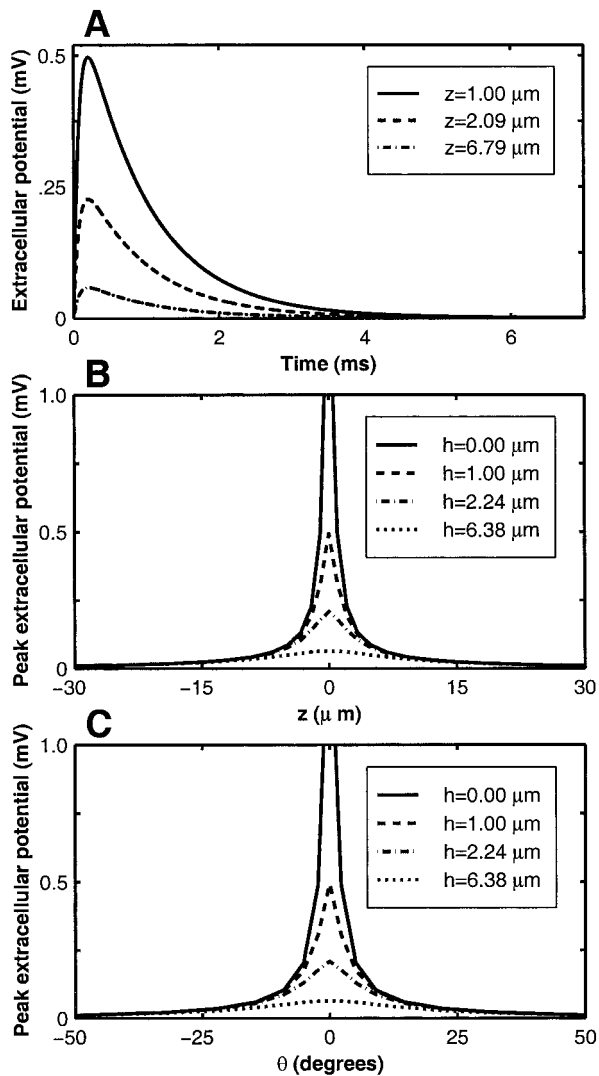
FIGURE 2 The magnitude of the extracellular quantal potential field, $V_e = -V_e$, following a quantal release at time $t = 0$ at the point $\theta = 0$, $z = 0$. A gives the extracellular potential V_e as a function of time for $\theta = 0$ and for selected values of z. B shows the peak values attained by V_e for $\theta = 0$ at distance z along the fiber and at selected distances h from the fiber surface ($h = 0$ corresponds to the surface). C shows the peak values attained by V_e for $z = 0$ at angle θ around the fiber and at selected distances h from the fiber surface.

the styryl dye FM1–43 (Fig. 5 *A*). Three simultaneous recordings were therefore taken of the electrical signs of a quantal release within the field of recording of the three external electrodes, whether the quanta were generated spontaneously (Fig. 5, *Ba* and *Bb*) or after nerve stimulation (Fig. 5 *Bc*). The first configuration of the three extracellular electrodes involved their placement at <1 μm above the surface of the muscle fiber and in a line at right angles to a release site region delineated by a blob of FM1–43 staining; the electrodes were situated about 4 μm apart with the electrode closest to the release site separated from its center by approximately 2.5 to 3 μm or more (Fig. 6 *A*). This

configuration allowed estimates to be made of how the quantal potential field declines in the circumferential direction. Fig. 6 *B* shows that for a series of quantal releases, involving the three largest quantal fields measured by the electrode closest to the release site, there is in each case an approximate linear relation of gradient −1 between log-(MEPP amplitude; V_e) and log(distance), although some positive curvature is evident. Three additional experiments of the kind shown in Fig. 6 were performed. The average value of the highest estimates of the gradient for each of three MEPPs in any one experiment was determined, yielding an average of this value over the three experiments of 0.99 ± 0.02.

The second configuration of electrodes consisted of these placed in a triangular array about the release sites of a terminal branch and separated from each other by about 5 μm (Fig. 5, *A* and *C*). In this case the triangulation algorithm described in Methods could be applied to the recorded excitatory postsynaptic potentials (EPSPs, Fig. 7 *C*) and this used to ascertain the site of release of a quantum, based on the assumption that a linear relation of gradient −1 exists between log(MEPP amplitude; V_e) and the logarithm of the distance between an electrode and site of release of the quantum. Comparison between the sites of quantal release along a terminal branch predicted by this method (Fig. 7 *B*) and the position of such sites determined by staining with FM1–43 (Fig. 7 *A*) showed that the former agreed with the latter. Both EPSPs and MEPPs were observed to originate exclusively from the regions of the nerve terminal that contained FM1–43 blobs in all experiments (16 blobs on 7 terminal branches), so that all release was from within these regions and there was no release between such regions.

This provided some independent evidence for the quantitative relation between the logarithm of the size of the quantal potential field and the logarithm of the distance from the origin of the field, ascertained both theoretically and experimentally above. The observations suggest that the departure from linearity of this relation observed both theoretically and experimentally is not so great as to produce major errors.

Fig. 8 shows, for comparison, experimentally recorded potentials together with the corresponding potentials calculated numerically. Fig. 8, *A* and *C*, show experimental MEPPs recorded intracellularly and extracellularly, respectively; *B* and *D* give the corresponding calculated waveforms. The good agreement provides further confirmation for the accuracy of the present theory.

DISCUSSION

Cable properties and the quantal current field in a volume conductor

Several inquiries have been made concerning the current field strength inside a spherical neuron and in the syncytial
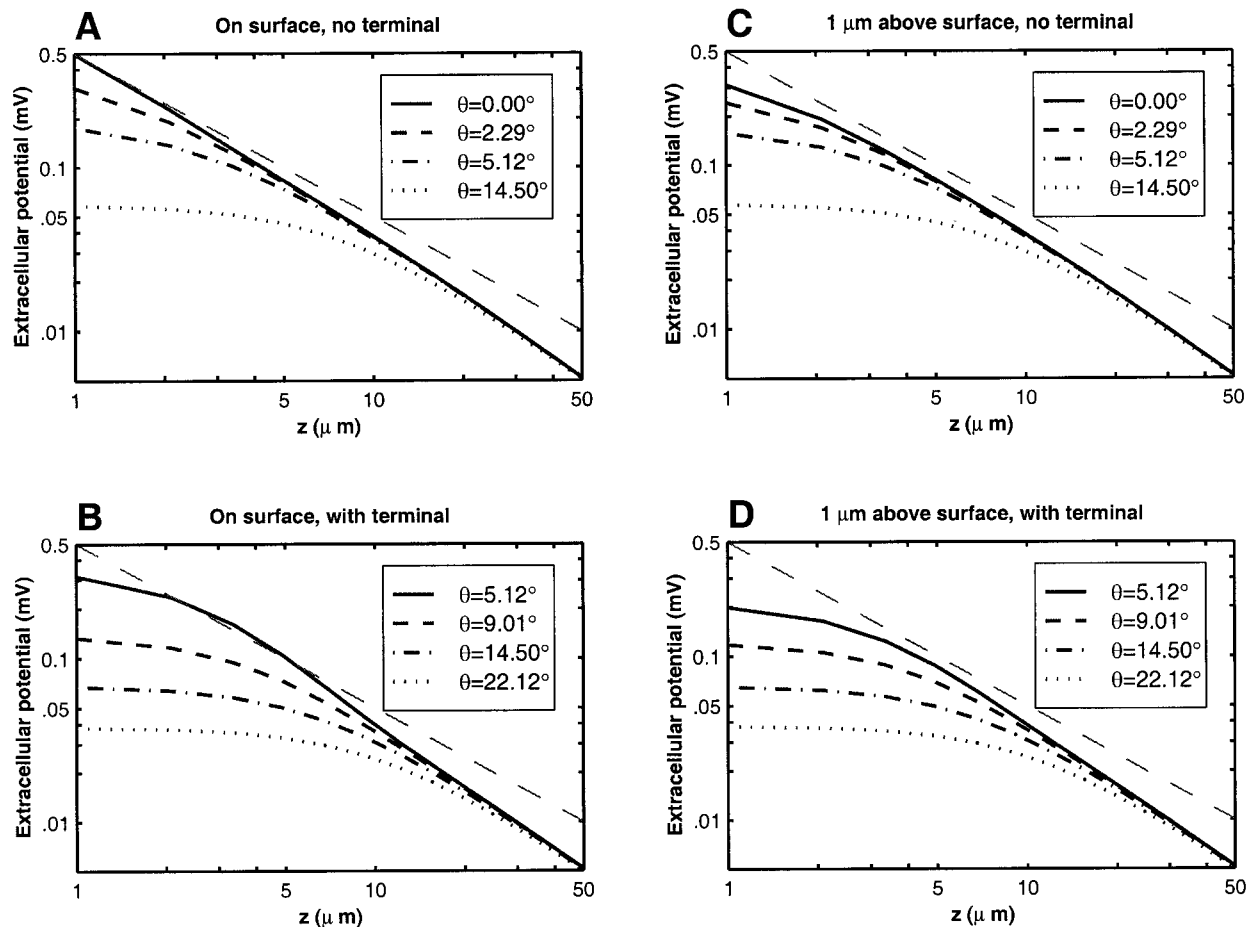
FIGURE 3 The magnitude of the extracellular quantal potential field, V_e, following a quantal release at time $t = 0$ at the point $\theta = 0$, $z = 0$, in the absence (A and C) and in the presence (B and D) of an overlying terminal branch and its associated Schwann cell covering (log-log plots). A shows the peak attained by $|V_e|$ at the surface of the muscle fiber as a function of the distance z along the fiber and for selected angles θ around the circumference of the fiber. B shows the same as in A, but in the presence of the terminal. C and D repeat A and B, respectively, except that V_e is given at a distance of 1 μm above the surface of the muscle fiber. In B and D the terminal excludes values of $\theta <$ about 3°. In each panel the fine broken straight line indicates a gradient of −1.

bidomain of smooth muscle and cardiac muscle. Eisenberg and his colleagues have considered the problem of how current flows from a point source in a spherical cell to give rise to changes in the resting membrane potential (Engel et al., 1972). The convergence of current results in a non-uniform spatial variation of the membrane potential, with a steep gradient of potential near the current source that reaches a steady state with a time constant much smaller than the membrane time constant. A similar phenomenon occurs if the current source is at the membrane, as shown in the present work, although in the idealization of the physical situation modeled here, the membrane potential very near the source goes to infinity as the current lines are forced to condense into a very small area at the current source and sink.

Previous attempts have been made to determine the relation between the excitatory junction potential recorded with a loose-patch electrode placed over a sympathetic varicosity

and the underlying current. This involves solving the time-dependent equations relating voltage and current in a three-dimensional syncytium of smooth muscle following a point source current injection into a syncytium, using the bidomain model of the electrical syncytium (Engel et al., 1972; Muler and Markin, 1977; Peskoff, 1979a,b; Tung, 1979). However, the bidomain equations describe a situation in which two domains, the intracellular and extracellular, are superimposed in the same region of space. Furthermore, they do not consider the case of the syncytial bidomain in a volume conductor, so that no solution is offered to the problem of how current flows in the three dimensions about a current source.

Properties of the quantal potential field

An approximately inverse relation was found to exist between the size of the quantal potential field at different
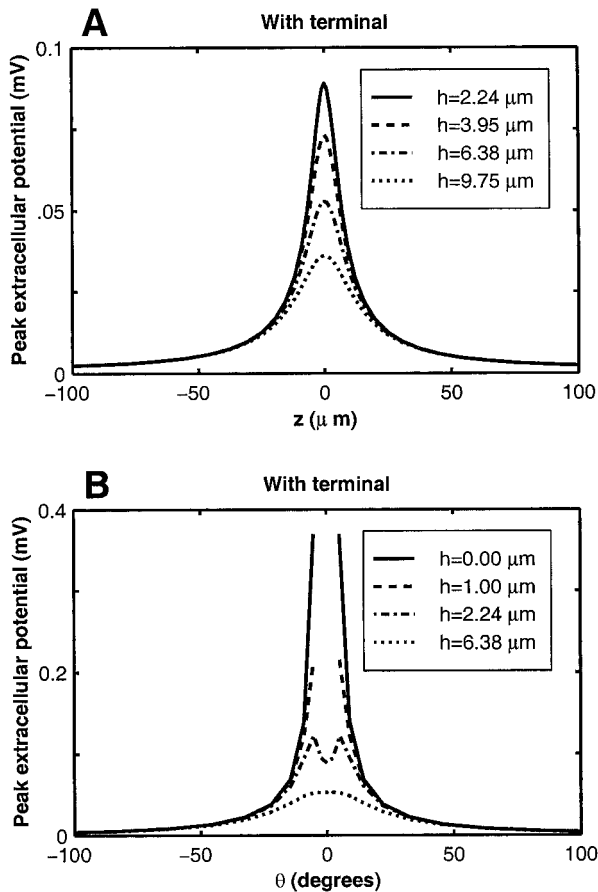
FIGURE 4 The magnitude of the extracellular quantal potential field V_e following a quantal release at time $t = 0$ at the point $\theta = 0$, $z = 0$ in the presence of an overlying terminal branch and its associated Schwann cell covering. *A* shows the peak values attained by V_e for $\theta = 0$ at distance z along the fiber and at selected distances h from the fiber surface ($h = 0$ corresponds to the surface but because of the terminal only values for $h >$ 2 μm are meaningful for $\theta = 0$). *B* shows the peak values attained by V_e for $z = 0$ at angle θ around the fiber and at selected distances h from the fiber surface. (For $h < 2$ μm, only values for $\theta >$ about 3° are meaningful.)

distances from its source; that is, the gradient of the log of the magnitude of the potential field (V_e) when plotted against the log of the distance (d) from the source was approximately -1.0 at distances greater than a few microns from the source. (It is interesting in this regard to note that the solution of Laplace's equation in spherical coordinates in the absence of any obstruction also gives a 1/d relation.) However, as has been noted, there is positive curvature in this relation until 10 μm beyond the source. Zefirov et al. (1990) obtained theoretically a 1/d falloff in the potential by modeling current release on an infinite plane membrane (see also the Appendix to this paper). However, it is not a priori evident that their result is applicable in the case of a cylindrical membrane; indeed, the present calculation shows that the 1/d falloff is only approximately true and then only over a limited, though physiologically significant, range of values of d. In the experimental work, a comparison was made

between the predictions of the position of these sources based on the inverse relation and independent verification of these positions using FM1–43 staining. Given this inverse relation, Fig. 3 *D* shows that an electrode placed 1 μm above the surface of a muscle fiber and about 2 μm in the circumferential direction from the site of a quantal release might record a quantal potential field value (V_e) of about 200 μV; this then attenuates to about 40 μV in a longitudinal distance of 10 μm, that is to one-quarter over this distance. Larger quantal events will, of course, attenuate at the same rate. This rate of attenuation is the same as that measured experimentally by a number of different authors (Katz and Miledi, 1965a,b; Wernig, 1975, 1976; Bennett and Lavidis, 1982), as mentioned in the Introduction. A quantal potential field of about 20 μV could just be detected with an appropriate noise level, which according to Fig. 3 will occur at 20 μm from the source of a quantal event. This agrees with the experimental work that shows that if an electrode is more than 15 to 20 μm from the source, then the MEPC is not recorded at all (Katz and Miledi, 1965a,b; Wernig, 1975, 1976; Bennett and Lavidis, 1982).

Combined intracellular and extracellular electrode determinations of quantal potential fields

The technique of locating the origins of MEPPs with two intracellular electrodes placed so that they straddle the endplate in the longitudinal direction was introduced by Gunderson et al. (1981). This approach was subsequently used by others for the purpose of determining if non-uniformities exist in the frequency and amplitude of MEPPs at different sites within the endplate (Tremblay et al., 1984; D'Alonzo and Grinnell, 1985; van der Kloot and Cohen, 1985; Robitaille et al., 1987; Robitaille and Tremblay, 1989). The technique involves comparing either the peak sizes of the MEPPs or their voltage-time integrals as recorded by each of the intracellular electrodes. The information from these measurements, together with a determination of the length constant of the fibers using brief current pulses, is then utilized in the standard cable equations (Jack et al., 1975) to give estimates of the positions of single quantal releases. Recently, van der Kloot and Naves (1996) used the two intracellular electrode approach to record MEPPs and ascertain their site of generation while at the same time recording the quantal releases with an extracellular electrode. By matching those MEPPs that were simultaneously recorded with the intracellular and extracellular electrodes, an estimate could be made of the distances over which the extracellular electrode could record a MEPP originating at different sites. In this way determinations were made of the extent of the quantal potential field along the length of the muscle fiber that were of the order of several hundreds of microns. These results are at least an order of magnitude greater than previous estimates of the extent of the quantal
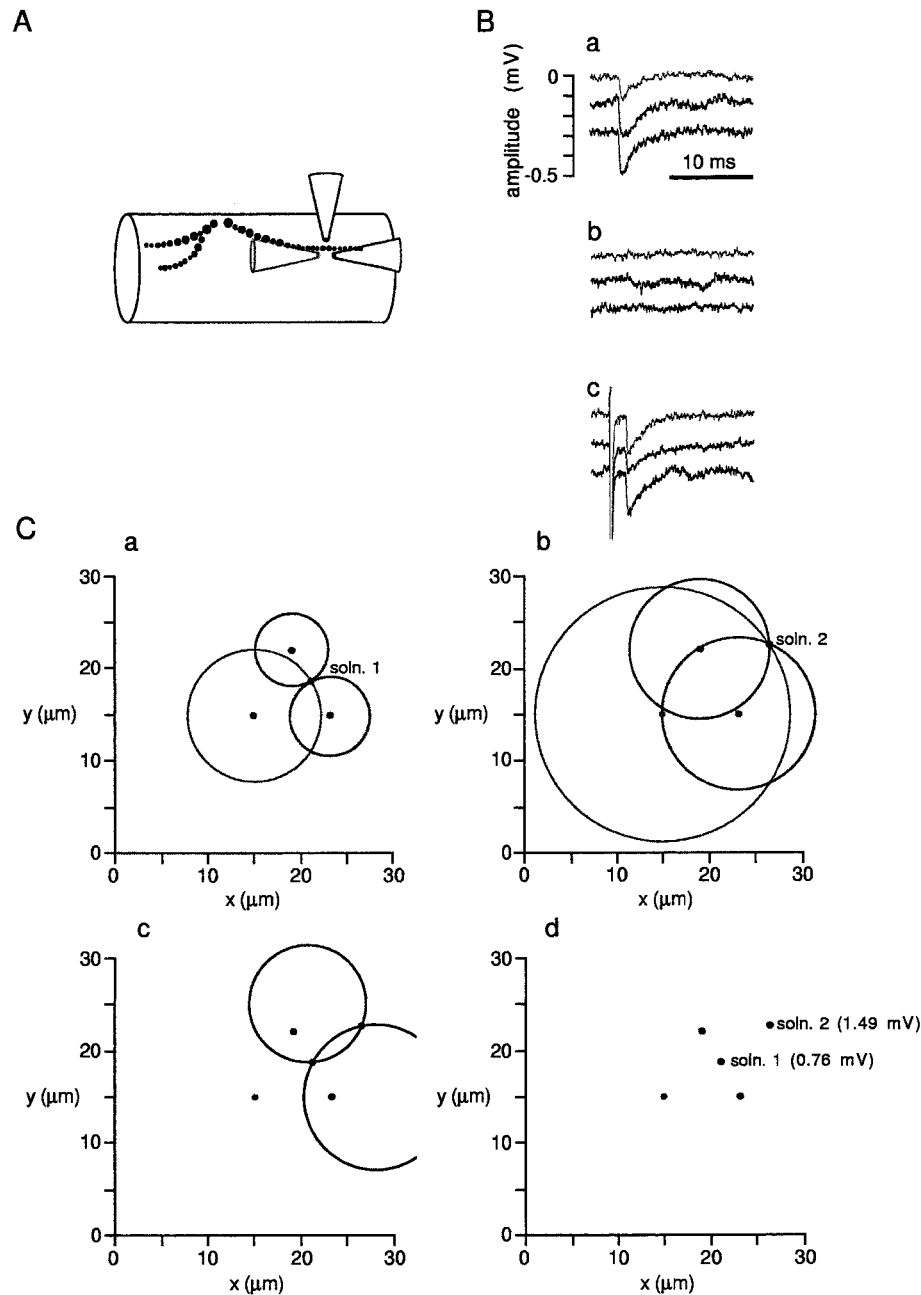
FIGURE 5   Experimental determination of the point of origin and amplitude of a quantal event. *A* shows a schematic representation of the recording positions for three extracellular microelectrodes relative to a motor nerve terminal branch. The position of the terminal is shown by the black spots that indicate discrete clusters of vesicles revealed through FM1–43 staining (blobs). *B* gives three extracellular electrode traces showing a miniature endplate potential (MEPP) that occurs within the radius of detection of the extracellular electrodes (*Ba*), and a MEPP outside this radius (*Bb*). In *Bc*, a stimulus to the nerve trunk evokes an endplate potential (EPP) from within the radius of detection. In *Ba*, the amplitude of the MEPP as measured by each electrode is 0.109, 0.183, and 0.197 mV, respectively. The ratio of these amplitudes yields a ratio of distances, from the electrodes to the source of the MEPP, of 1.68:1.00:0.93 respectively, assuming that the MEPP amplitude recorded at each microelectrode is inversely proportional to its distance from the source of the MEPP (see text). *Ca* illustrates one possible location for the source of the MEPP at the intersection of three circles with radii in the ratio of 1.68:1:0.93 centered on the electrodes. (The axes, *x* and *y*, define the spatial dimensions in the plane of the three electrode tips, which are indicated by the dots.) *Cb* illustrates the second possible location at the intersection of the three circles whose radii are also in the ratio 1.68:1:0.93. *Cc* shows another approach for determining the source of the MEPP. This involves calculating the locus of possible source locations determined by consideration of the MEPPs recorded by just two microelectrodes in turn. The intersection of the two sets of loci gives two solutions to the problem, in the same way as the approach illustrated in *Ca* and *Cb*. Further criteria must be used to decide which of the two solutions is correct. The assumption that the event amplitude recorded at each microelectrode is inversely proportional to the distance from the source of the event allows an estimate to be made of the amplitude of an event as it would be measured at a distance of 1 μm from the site of its generation. In this case the amplitude of solution 1 is 0.76 mV while solution 2 is 1.49 mV (*Cd*). The criterion for discriminating the most probable solution is formalized in the Methods section.
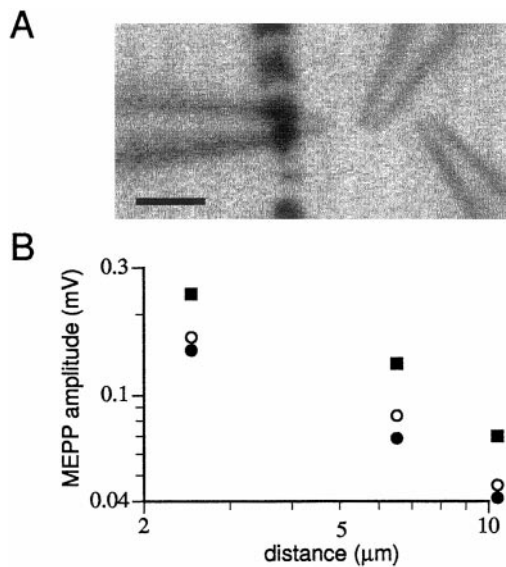
A

B

FIGURE 6 Experimental measurement of extracellular quantal potential fields in the vicinity of release sites of a terminal branch. *A* shows the tips of three extracellular electrodes placed in a configuration at right angles to a terminal branch and opposite release sites delineated by FM1–43 staining; the distances between each electrode is about 4 μm with the electrode closest to the release site at a distance of about 2.5 μm. *B* gives the relation between the logarithm of the peak amplitude of a MEPP recorded with each of the three electrodes and the logarithm of their distance away from the release site in *A*. Only the recordings that gave the largest MEPP sizes and the steepest gradients when plotted on these coordinates were used; these had a gradient of about −1.

potential field or those of the present work (Katz and Miledi, 1965a,b; Wernig, 1975, 1976; Bennett and Lavidis, 1982). One explanation for these discrepancies relates to the size of the volume conductor, that is, to the height of the solution bathing the nerve terminal above the nerve terminal. As this decreases, the quantal current field is extended in the longitudinal (z) direction. The relation between the depth of the solution bathing the nerve terminal and the longitudinal spread of the quantal voltage field is shown in Fig. 9. Once the solution depth is reduced to about 50 μm, the longitudinal field is such that MEPCs of 20 μV can be recorded at distances of several hundred microns from the source.

CONCLUSION

Solutions have been obtained for the equations describing the potential field generated in a volume conductor around a synapse after the release of a quantum of transmitter. These show that the field declines approximately as the inverse of the distance from the source at distances greater than about 4 μm, so that the field is severely attenuated within about 10 μm from the source. This result has been vindicated experimentally using three external electrodes to record the MEPCs. The degree of attenuation of the field
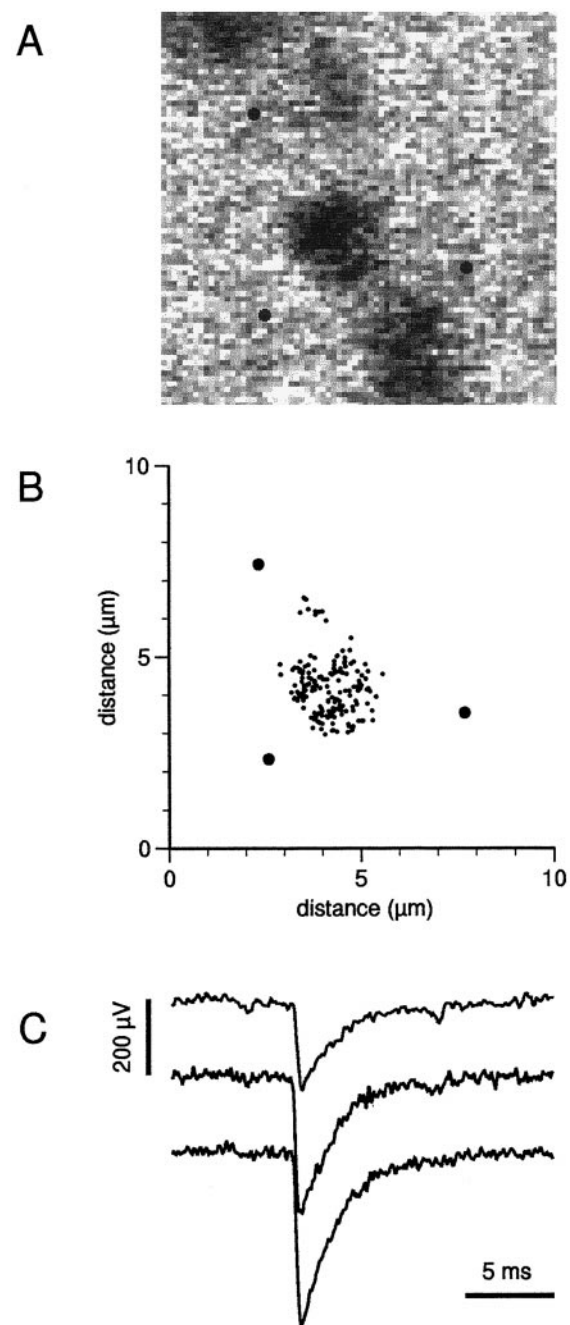
A

B

C

FIGURE 7 Experimental comparison between the sites of quantal release determined by electrical means and that using FM1–43 staining. *A* shows a terminal branch with release sites delineated by the blobs of FM1–43 staining; the positions of the three extracellular electrodes with respect to the terminal branch are indicated by *filled circles*. *B* gives the sites of quantal release determined using a triangulation algorithm based on the inverse relation between the amplitude of the quantal potential field about a release site and the distance from the site; the high frequencies of quantal release coincide with the centers of the FM1–43 stained blob in *A*; only sites of quantal release determined as falling within the triangle have been plotted. *C* shows examples of simultaneous recordings made with the three extracellular electrodes of a single MEPP.
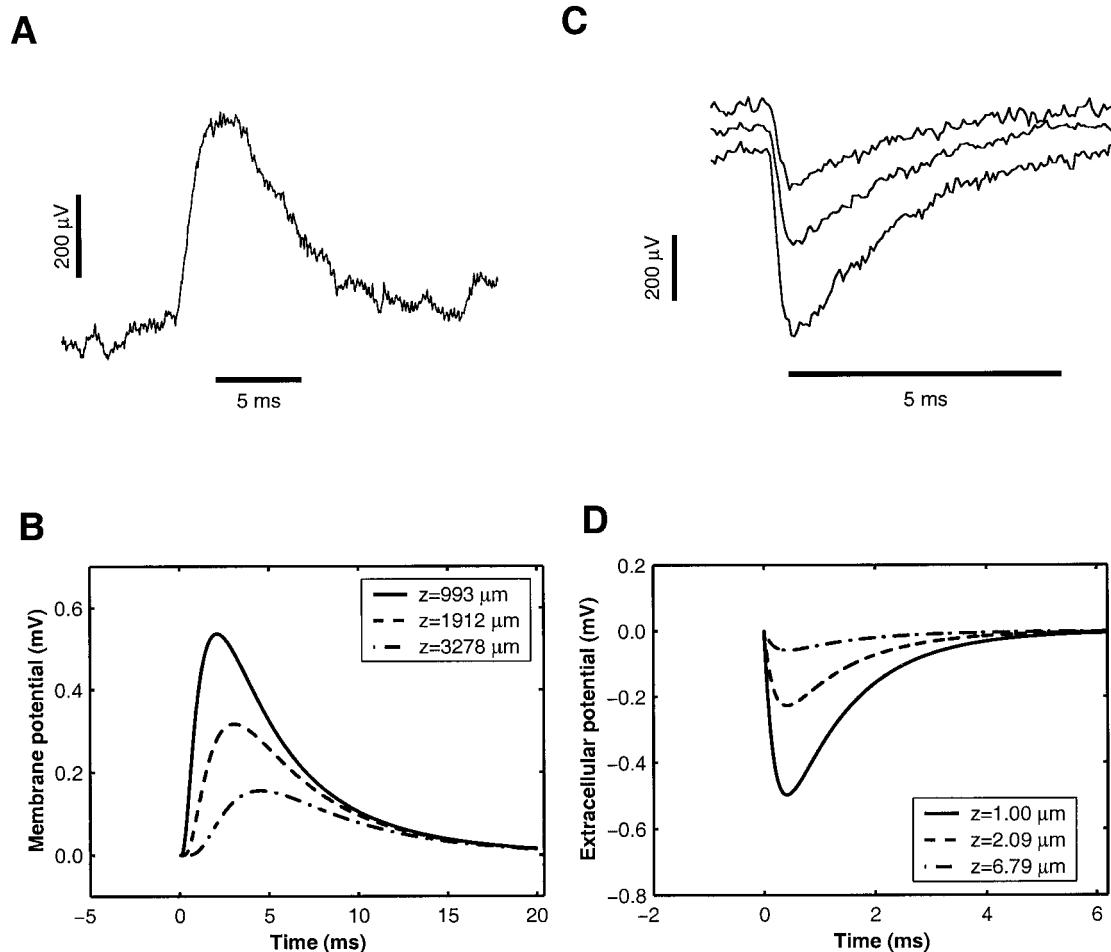
FIGURE 8   Comparison of experimental and theoretical waveforms. *A* shows a typical experimental MEPP recorded with an intracellular electrode and *B* gives the calculated intracellular MEPP potential at three different distances from the release site. *C* shows three experimental MEPPs as recorded with an extracellular electrode and *D* gives the calculated extracellular MEPP at three different distances from the release site. In each case, the experimental and theoretical graphs are scaled identically to facilitate comparison.

can be modified by changing the extent of the volume conductor.

APPENDIX: Effect of finite source size.

Eq. 3 mimics synaptic transmission by a point current source placed at the point $(r, \theta, z) = (a, 0, 0)$. A consequence of this is that the exact solution to Eqs. 2 and 3 is infinite at this point. (See chapter 5 of Jack et al. (1975) for a discussion of this effect in physiological systems. More generally, it is related to the fact that the Green's function for diffusion in more than one dimension is singular; see, e.g., Morse and Feshbach, 1953.) The numerical solution to Eqs. 2 and 3 is finite everywhere, but is unrealistically large at the source point, where its magnitude depends on the spacing used in the integration grid.

These problems arise because a physically extended source, the receptor patch, has been idealized to a point. To investigate the validity of this approximation it is desirable to compare the solutions for an extended source and for a point source. Such a comparison is not feasible for the cylinder case, but it is for the simpler case of a plane membrane. Specifically, we solve analytically the problem of synaptic transmission from an extended source on a infinite plane membrane and compare this solution

with the analytic solution for a point source and with the numerical solution for a point source.

The plane membrane is taken to lie in the plane $z = 0$ and separate the space into exterior $(z > 0)$ and interior $(z < 0)$ regions. Eq. 1 is

$$\frac{\partial^2 V}{\partial x^2} + \frac{\partial^2 V}{\partial y^2} + \frac{\partial^2 V}{\partial z^2} = 0, \quad z \neq 0. \tag{5}$$

We are interested only in the steady-state solution and Eq. 3 is replaced by

$$\frac{1}{R_i} \frac{\partial V}{\partial z}\bigg|_{z=0-} = \frac{1}{R_e} \frac{\partial V}{\partial z}\bigg|_{z=0+} = -\frac{V_m}{R_m} + I(x, y) \tag{6}$$

where $I(x, y)$ is the extended current source, taken to be a constant current with a spatial profile given by the Gaussian

$$I(x, y) = I_0 \frac{1}{2\pi\sigma^2} \exp(-\rho^2/2\sigma^2), \tag{7}$$

where $\rho = \sqrt{x^2 + y^2}$ and σ is a parameter determining the spatial spread. In the limit $\sigma \to 0$, $I(x, y) \to I_0 \delta(x)\delta(y)$, which is the point-source case.
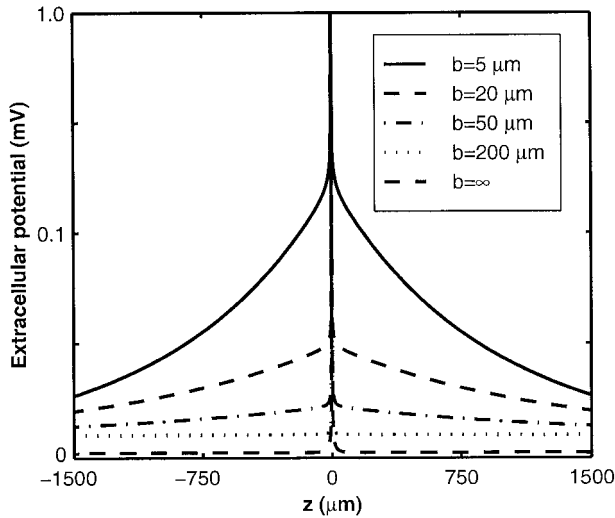
FIGURE 9 The effect of decreasing the size of the volume conductor on the extracellular quantal potential field V_e. The muscle fiber is contained in another coaxial cylinder of radius $b > a$ with extracellular fluid in the region $a < r < b$. Shown are the peak values attained by V_e for $\theta = 0$ at distance z along the fiber and at its surface for selected values of b in the range from 5 to 200 μm. Also shown is the unrestricted case (*lower broken line*).
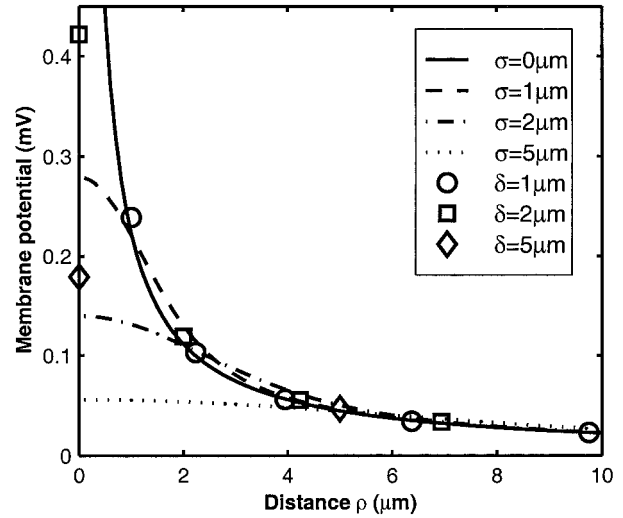

FIGURE 10 The membrane potential due to an extended source as a function of distance from the source. The source has the Gaussian profile given by Eq. 7 and is centered at the point $(x, y, z) = (0, 0, 0)$ on a flat membrane of infinite extent occupying the plane $z = 0$. $I_0 = 1$ nA and the rest of the parameters are as in Table 1. The *solid line* gives the membrane potential for a point source ($\sigma = 0$); the *broken lines* are for extended sources of various sizes ($\sigma > 0$), calculated using Eq. 8. The symbols give the results of numerical calculations, using a point source and various grid sizes, as specified by the initial grid spacing δ. (Because an expanding grid is used, δ increases with distance from the source.)

Eqs. 5 and 6, with input current Eq. 7 can be solved exactly using, for example, Hankel transform methods (Carrier et al., 1966). The result for the membrane potential is

$$V_m(\rho) = \frac{I_0}{2\pi}(R_i + R_e)\int_0^\infty \zeta J_0(\rho\zeta)\frac{1}{\zeta + \mu}\exp(-\zeta^2\sigma^2/2)d\zeta$$

(8)

where $\mu = (R_i + R_e)/R_m$ and $J_0(x)$ is a Bessel function of order zero. (For $\sigma = 0$, Eq. 8 is related to a result of Zefirov et al., 1990.) Since $\mu \ll 1$, for small σ Eq. 8 can be approximated at the source point $\rho = 0$ by

$$V_m(0) \approx \frac{I_0}{2\pi}(R_i + R_e)\sqrt{\frac{\pi}{2}}\frac{1}{\sigma}$$

(9)

showing that the membrane potential diverges as $1/\sigma$ as $\sigma \to 0$.

Fig. 10 shows $V_m(\rho)$ as a function of ρ for various values of σ. The solid line is the point-source case; broken lines are for $\sigma = 1$, 2, and 5 μm. It is seen that in each case the broken lines and the solid line are very close for all distances $\rho > \sigma$, but deviate considerably for smaller distances. This means that the analytic point-source solution is a good approximation to the extended source case for distances of at least σ from the center of the source. Also shown are the results of numerical calculations of the membrane potential due to the point source, using various grid spacings δ. These show that δ performs much the same function in the numerical case as σ did in the analytic case, and the numerical results should be meaningful for $\rho > \delta$.

These results are for a simplified model (plane membrane, constant current input), but there seems to be no reason why the cylindrical case, even for a time-dependent input, should not exhibit a similar relation between the extended source and the point source cases. The figures in this paper show potentials to within one grid spacing of the source; however, in the applications to the experimental cases only data calculated at distances of several grid points away is needed, so it is expected that there is negligible error resulting from the point-source idealization.

REFERENCES

Adrian, R. H., and W. Almers. 1973. Measurement of membrane capacity in skeletal muscle. *Nature (New Biol.).* 242:62–64.

Altman, K. W., and R. Plonsey. 1988. Development of a model for point source electrical fiber bundle stimulation. *Med. Biol. Eng. Comput.* 26:466–476.

Bennett, M. R., P. Jones, and N. A. Lavidis. 1986. The probability of quantal secretion along visualized terminal branches at amphibian (Bufo marinus) neuromuscular synapses. *J. Physiol.* 379:257–274.

Bennett, M. R., and N. A. Lavidis. 1982. Variation in quantal secretion at different release sites along developing and mature motor terminal branches. *Brain Res.* 281:1–9.

Bennett, M. R., W. G. Gibson, and R. R. Poznanski. 1993. Extracellular current flow and potential during quantal transmission from varicosities in a smooth muscle syncytium. *Phil. Trans. Roy. Soc. Lond. B.* 342:89–99.

Bennett, M. R., and W. G. Gibson. 1995. On the contribution of quantal secretion from close-contact and loose-contact varicosities to the synaptic potentials in the vas deferens. *Phil. Trans. Roy. Soc. Lond.* 347:187–204.

Bennett, M. R., L. Farnell, W. G. Gibson, and N. A. Lavidis. 1997. Synaptic transmission at visualized sympathetic boutons: stochastic interaction between acetylcholine and its receptors. *Biophys. J.* 72:1595–1606.

Bennett, M. R., L. Farnell, and W. G. Gibson. 1999. Cable analysis of a motor-nerve terminal branch in a volume conductor. *Bull. Math. Biol.* 61:1–17.

Betz, W. J., and G. S. Bewick. 1993. Optical monitoring of transmitter release and synaptic vesicle recycling at the frog neuromuscular junction. *J. Physiol.* 460:287–309.

Carrier, G. F., M. Krook, and C. E. Pearson. 1966. Functions of a Complex Variable: Theory and Technique. McGraw-Hill Book Co., New York.

Clark, J., and R. Plonsey. 1968. The extracellular potential field of the single active nerve fiber in a volume conductor. *Biophys. J.* 8:842–864.

D'Alonzo, A. J., and A. D. Grinnell. 1985. Profiles of evoked release along the length of frog motor nerve terminals. *J. Physiol.* 359:235–258.

del Castillo, J., and B. Katz. 1954. Quantal components of the end-plate potential. *J. Physiol.* 124:560–573.

del Castillo, J., and B. Katz. 1956. Localization of active spots within the neuromuscular junction of the frog. *J. Physiol.* 132:630–649.

Eisenberg, R. S., and R. S. Johnson. 1970. Three-dimensional electrical field problems in physiology. *Prog. Biophys. Mol. Biol.* 20:1–65.

Engel, E., V. Barcilon, and R. S. Eisenberg. 1972. The interpretation of current-voltage relations recorded from a spherical cell with a micro-electrode. *Biophys. J.* 12:384–403.

Fatt, P., and B. Katz. 1952. Spontaneous subthreshold activity at motor nerve endings. *J. Physiol.* 117:109–128.

Forti, L., M. Bossi, A. Bergamaschi, A. Villa, and A. Malgaroli. 1997. Loose-patch recordings of single quanta at individual hippocampal synapses. *Nature.* 388:874–878.

Gage, P. W., and C. M. Armstrong. 1968. Miniature end-plate currents in voltage-clamped muscle fiber. *Nature.* 218:363–365.

Gunderson, C. G., B. Katz, and R. Miledi. 1981. The reduction of endplate responses by botulinum toxin. *Proc. Roy. Soc. Lond. B.* 213:489–493.

Henery, R., W. G. Gibson, and M. R. Bennett. 1997. Quantal currents and potential in the three-dimensional anisotropic bidomain model of smooth muscle. *Bull. Math. Biol.* 59:1047–1075.

Hodgkin, A. L., and W. A. H. Rushton. 1946. The electrical constants of a crustacean nerve fiber. *Proc. Roy. Soc. Lond. B.* 133:444–479.

Hodgkin, A. L., and S. Nakajima. 1972a. The effect of diameter on the electrical constantas of frog skeletal muscle fibres. *J. Physiol.* 221:105–120.

Hodgkin, A. L., and S. Nakajima. 1972b. Analysis of the membrane capacity in frog muscle. *J. Physiol.* 221:121–136.

Jack, J. J. B., Noble, D., and R. W. Tsien. 1975. Electric Current Flow in Excitable Cells. Oxford University Press, Oxford.

Katz, B. 1966. Nerve, Muscle, and Synapse. McGraw-Hill, New York.

Katz, B., and R. Miledi. 1965a. Propagation of electric activity in motor nerve terminals. *Proc. Roy. Soc. Lond. B.* 161:453–482.

Katz, B., and R. Miledi. 1965b. Release of acetylcholine from a nerve terminal by electric pulses of variable strength and duration. *Nature.* 207:1097–1098.

Katz, B., and S. Thesleff 1957. On the factors which determine the amplitude of the "miniature end-plate potential". *J. Physiol. (Lond.).* 137:267–278.

Lavidis, N. A., and M. R. Bennett. 1992. Probabilistic secretion of quanta from visualized sympathetic nerve varicosities in mouse vas deferens. *J. Physiol.* 454:9–26.

Macleod, G. T., J. B. Gan, and M. R Bennett. 1999. Vesicle-associated proteins and quantal release at single active zones of amphibian (Bufo marinus) motor-nerve terminals. *J. Neurophysiol.* 82:1133–1146.

Magleby, K. L., and C. F. Stevens. 1972. A quantitative description of end-plate currents. *J. Physiol.* 223:173–197.

Malmivuo, J., and R. Plonsey. 1995. Bioelectromagnetism. Oxford University Press, New York.

Morse, P. M., and H. Feshbach. 1953. Methods of Theoretical Physics. McGraw-Hill, New York.

Muler, A. L., and V. S. Markin, 1977. Electrical properties of anisotropic neuromuscular syncytia. III. Steady state of front of excitation. *Biofizika.* 22:671–675.

Peskoff, A. 1979a. Electric potential in three-dimensional electrically syncytial tissues. *Bull. Math. Biol.* 41:163–181.

Peskoff, A. 1979b. Electric potential in cylindrical syncytia and muscle fibres. *Bull. Math. Biol.* 41:183–192.

Peskoff, A., and R. S. Eisenberg. 1975. The time-dependent potential in a spherical cell using matched asymptotic expansions. *J. Math. Biol.* 2:277–300.

Peskoff, A., and D. M. Ramirez. 1975. Potential induced in a spherical cell by an intracellular point source and an extracellular point sink. *J. Math. Biol.* 2:301–316.

Pickard, W. F. 1971a. Electrotonus on a cell of finite dimensions. *Math. Biosci.* 10:201–13.

Pickard, W. F. 1971b. The spatial variation of plasmalemma potential in a spherical cell polarized by a small current source. *Math. Biosci.* 10:307–28.

Rattray, F. 1986. Analysis of models for external stimulation of axons. *IEEE Trans. Biomed. Eng.* 33:974–977.

Rattray, F. 1987. Ways to approximate current-distance relations for electrically stimulated fibers. *J. Theor. Biol.* 125:339–349.

Rattray, F. 1989. Analysis of models for extracellular fiber stimulation. *IEEE Trans. Biomed. Eng.* 36: 676–682.

Robitaille, R., and J. P. Tremblay. 1989. Frequence and amplitude gradients of spontaneous release along the length of the frog neuromuscular junction. *Synapse.* 3:291–307.

Robitaille, R., J. P. Tremblay, and G. Grenon. 1987. Interrelation between MEPP amplitude and MEPP frequency in different regions along the frog neuromuscular junction. *Brain Res.* 408:353–358.

Stephanova, D., N. Trayanova, A. Gydikov, and A. Kossev. 1989. Extracellular potentials of a single myelinated nerve fiber in an unbound volume conductor. *Biol. Cybern.* 61:205–210.

Thomson, P. C., N. A. Lavidis, J. Robinson, and M. R. Bennett. 1995. Probabilistic secretion of quanta at somatic motor-nerve terminals: the fusion-pore model, quantal detection and autoinhibition. *Phil. Trans. Roy. Soc. Lond. B.* 349:197–214.

Trayanova, N., C. S. Henriquez, and R. Plonsey. 1990. Extracellular potentials and currents of a single active fiber in a restricted volume conductor. *Ann. Biomed. Eng.* 18:219–238.

Tremblay, J. P., R. Robitaille, and G. Grenon. 1984. Distribution of spontaneous release along the frog neuromuscular junction. *Neurosci. Lett.* 51:247–252.

Tuckwell, H. C. 1988. Introduction to Theoretical Neurobiology. Cambridge University Press, Cambridge.

Tung, L. 1979. Three-dimensional cable theory: a bidomain model. *Biophys. J.* 25:214a.

van der Kloot, W., and I. Cohen. 1985. Localizing the site of generation of uni-quantal endplate potentials using two intracellular microelectrodes. *Neurosci. Lett.* 62:57–62.

van der Kloot, W., and L. A. Naves. 1996. Localizing quantal currents along frog neuromuscular junctions. *J. Physiol.* 497:189–198.

Wernig, A. 1975. Estimates of statistical release parameters from crayfish and frog neuromuscular junctions. *J. Physiol.* 244:207–221.

Wernig, A. 1976. Localization of active sites in the neuromuscular junction of the frog. *Brain Res.* 118:63–72.

Zefirov, A. L., T. V. Benish, and N. F. Fatkullin. 1990. [The detection of the sites of mediator release in a motor nerve ending]. [Russian]. *Neirofiziologiya.* 22:309–318.

Zefirov, A., T. Benish, N. Fatkullin, S. Cheranov, and R. Khazipov. 1995. Localization of active zones. *Nature.* 376:393–394.